TABLE I
RIPPLE $\mathcal{R}$ IN dB, (a) FOR NARROW HEAD, AND (b) FOR BROAD HEAD FOR SELECTED VALUES OF SHIELD PARAMETERS, c_s/b AND b_s/b

(a) $w/b=0.1$, $w_s/b=0.05$

c_s/b	b_s/b	R
0.05	1.0	14.0
"	1.1	16.7
"	1.5	24.7
0.10	1.0	12.7
"	1.1	14.0
"	1.2	15.3
"	1.3	16.5
"	1.4	17.3
"	1.5	17.5*
0.15	"	14.5
0.20	"	12.9
0.25	"	11.8
0.30	1.1	10.4
"	1.5	11.1
∞	0	8.8†

(b) $w/b=0.5$, $w_s/b=0.5$

c_s/b	b_s/b	R
0.15	1.5	8.8
0.25	1.0	7.2
"	1.5	7.8
0.50	1.0	6.6
∞	0	5.3†

*Also obtain same result within .1 dB if w_s/b is increased or decreased by a factor of 10.

†i.e., unshielded.

6(b)). The same phenomenon occurs if the clearance is fixed and the shield length is increased (Fig. 7). Table I contains the ripple for these geometries and several others not illustrated.

Summarizing these findings for side-shielded heads we find the following.

1) Ripple increases for a fixed clearance if the shield length becomes much longer than the head length $b_s > b$.
2) For a fixed shield length (even $b_s \simeq b$) the ripple can increase if the clearance is small enough.
3) Ripple is virtually independent of shield width w_s.

IV. Conclusion

It has been shown how the ripple and peak locations change with track width for an unshielded rectangular head. Most conventional heads are better approximated with zero width than infinite width on the basis of ripple. Thin-film heads, however, are well-approximated as infinite width heads.

Both narrow tracks and close proximity of long shields can increase the ripple of a rectangular head considerably. By bevelling or rounding the outer edges of the head, this effect can be reduced but not entirely eliminated.

References

[1] D. A. Lindholm, "Long wavelength response of magnetic heads with beveled outer edges," *J.A.E.S.*, vol. 27, p. 542, 1979.
[2] —, "Reproduce characteristics of rectangular magnetic heads," *IEEE Trans. Magn.*, vol. MAG-12, p. 710, 1976.
[3] A. Wexler, "Some applications of the boundary element method to electrical engineering problems," in *Recent Advances in Boundary Element Methods*, C. A. Brebbia, Ed. London: Pentech Press, p. 405, 1978.
[4] C. J. Collie, "Magnetic fields and potentials of linearly varying current or magnetization in a plane-bounded region," in *Proc. COMPUMAG*, Mar. 1976, Oxford, England, p. 86.
[5] A. Kopal, *Numerical Analysis*. New York: Wiley, p. 408, 1955.
[6] M. Abramowitz and I. Stegun, Eds., *Handbook of Mathematical Functions*. New York: Dover, p. 480, 1965.

Measurement of Saturation Magnetostriction of a Thin Amorphous Ribbon by Means of Small-Angle Magnetization Rotation

KENJI NARITA, MEMBER, IEEE JIRO YAMASAKI, AND HIROTOSHI FUKUNAGA

Abstract—A new method was developed to measure the saturation magnetostriction of a thin amorphous ribbon. It is based on the use of small-angle magnetization rotation to measure the change in anisotropy field caused by the tensile stress. Measurements have been performed on Metglas 2826, 2605, and Co-Si-B amorphous ribbons. The maximum experimental error of the measurement was estimated to be about ±5 percent. It is shown that the sensitivity of the method depends on the shape anisotropy field. The estimated sensitivity was about 2×10^{-7} for Metglas 2826 ribbon with 1.8 mm × 40 μm × 12 cm in dimensions.

Manuscript received April 9, 1979; revised October 1, 1979.
The authors are with the Department of Electrical Engineering, Kyushu University, Hakozaki, Fukuoka 812.

Introduction

AMORPHOUS ALLOYS have been well-known to be attractive soft magnetic materials because of the absence of magnetocrystalline anisotropy. However, it has been found that their magnetic properties, such as coercive force and

0018-9464/80/0300-0435$00.75

permeability, strongly depend on the magnitude of magnetostriction. From this point of view, measurement of magnetostriction is important for the study of the amorphous ferromagnetic materials.

Saturation magnetostrictions of amorphous ribbons have been measured with the strain gauge method [1], [2] or with the capacitance method [3]. The thicknesses of splat-cooled amorphous ribbons obtained so far are limited to be less than 80 μm. Then these direct strain measuring methods require several pieces of specimens to be bonded together to relieve a reactive effect due to the strain gauge or the movable electrode. However, an accurate estimation of this reactive effect seems to be difficult.

In the present work the authors have designed a simple method of measuring the saturation magnetostriction of a thin amorphous ribbon by means of small-angle magnetization rotation, applying the anisotropy field measuring technique originally developed for the Ni-Fe electrodeposited wire [4]. Data are presented on Metglas 2826, 2605 ribbons with compositions of $Fe_{40}Ni_{40}P_{14}B_6$ and $Fe_{80}B_{20}$, made by Allied Chemical Corporation and $Co_{76.7}Si_{13.3}B_{10}$ with a negative magnetostriction.

Theory

In order to cause the small-angle magnetization rotation in the ribbon plane a small amplitude ac drive field $H_\perp$ and a dc bias field $H_\parallel$, which is high enough to produce magnetic saturation, are applied simultaneously perpendicular and parallel to the ribbon axis, respectively. A schematic presentation is shown in Fig. 1. The induced voltage due to the magnetization rotation in a sense coil wound around the ribbon axis is proportional to the time derivative of the ribbon axis component of magnetization, so that

$$e_{2f} = -N \cdot S \cdot \frac{d}{dt}(4\pi M_s \cos\theta), \tag{1}$$

where N is the number of winding of the sense coil, S is the cross sectional area of the ribbon, M_s is the saturation magnetization, and θ is the angle between the magnetization and the ribbon axis. If the amorphous alloy has an isotropic saturation magnetostriction constant λ_s, the applied tensile stress σ induces an uniaxitial anisotropy. The magnetization rotation angle can be derived by considering the equation for the total energy density E, which includes the magnetoelastic energy,

$$E = -H_\parallel M_s \cos\theta - H_\perp M_s \sin\theta + \tfrac{3}{2}\lambda_s \sigma \sin^2\theta + \tfrac{1}{2} M_s(N_\perp \sin^2\theta + N_\parallel \cos^2\theta), \tag{2}$$

where $N_\perp$ and $N_\parallel$ are the demagnetizing factors perpendicular (of course in the ribbon plane) and parallel to the ribbon axis, respectively. Solving θ by putting $-dE/d\theta = 0$,

$$\sin\theta = \frac{H_\perp}{H_\parallel + 3\lambda_s\sigma/M_s + M_s(N_\perp - N_\parallel)} \tag{3}$$

is obtained, where $\cos\theta = 1$ is assumed because of the small amplitude of the ac drive field. The drive field is sinusoidal, and

$$H_\perp = H_{\perp\max} \sin\omega t. \tag{4}$$

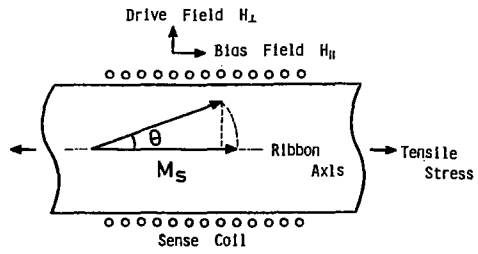

Fig. 1. Schematic presentation of small-angle magnetization rotation in ribbon plane.

Equation (1) and maximum rotation angle $\theta_{\max}$ can now be written as

$$e_{2f} = 2\pi N \cdot S \cdot M_s \cdot \omega \sin^2\theta_{\max} \sin 2\omega t, \tag{5}$$

$$\sin\theta_{\max} = \frac{H_{\perp\max}}{H_\parallel + H_k + H_s}, \tag{6}$$

where $H_k = 3\lambda_s\sigma/M_s$ and $H_s = M_s(N_\perp - N_\parallel)$ are the stress induced and shape anisotropy fields, respectively. As presented in (5), the angular frequency of induced voltage is 2ω. The amplitude is proportional to the square of sine of the maximum magnetization rotation angle, which depends on the dc bias field and the applied tensile stress. When the tensile stress is applied under the condition of the fixed ac drive field, the rotation angle decreases due to the increase in the anisotropy field H_k, which results in the decrease in e_{2f}. Such decrease in the rotation angle can be compensated by decreasing dc bias field $H_\parallel$ by $\Delta H_\parallel$ to keep e_{2f} constant, if

$$H_k = \Delta H_\parallel. \tag{7}$$

The value of saturation magnetostriction can be obtained for the given σ and the measured H_k as

$$\lambda_s = \frac{1}{3} \cdot \frac{H_k}{\sigma} \cdot M_s. \tag{8}$$

The above-mentioned analysis is based on the assumption that the magnetization rotates uniformly throughout the specimen inside the sense coil. In practice, it is considered that the rotation angle is nonuniform in magnitude because of the skin effect, high demagnetizing field at the ribbon edges, and probable nonuniform drive field. The effective $H_{\perp\max}$ and H_s in (6) differ at each point in the ribbon plane. For such nonuniformity, (5) should be written more accurately as

$$e_{2f} = 2\pi N \cdot \frac{1}{L} \cdot M_s \cdot \omega \int_v \sin^2\theta_{\max}\, dV \cdot \sin 2\omega t, \tag{9}$$

where L is the length of the sense coil, and V is the volume of the ribbon inside the sense coil. The integration is carried out over the whole volume of the ribbon. In the present method, the sum of $H_\parallel + H_k$ in (6) is kept constant by adjusting the value of $H_\parallel$, which leads to the constant value of integration for different values of tensile stress. Therefore, compensation of the anisotropy field by the bias field is not influenced by such nonuniformity of rotation angle.

The nonuniform magnetization rotation might be also caused by the presence of local anisotropy in the as-quenched amor-

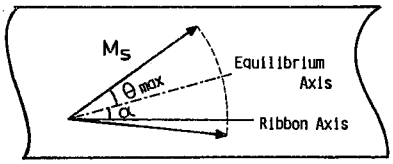

Fig. 2. Schematic presentation of small-angle magnetization rotation in ribbon plane, where α is angle between equilibrium axis of magnetization and ribbon axis.

phous ribbon. It has been reported that the anisotropy originates from the internal stress quenched-in during ribbon synthesis [5], [6]. It seems to be quite natural to consider that in the single domain state the magnetization is in the ribbon plane because of the large demagnetizing effect normal to the ribbon plane. Therefore we deal with the case where the equilibrium axis of magnetization rotation skews slightly from the ribbon axis only in the ribbon plane. A schematic presentation is shown in Fig. 2, where α is the skew angle of equilibrium axis. At the local anisotropy region, the induced voltage in the sense coil is obtained as

$$e = 2\pi N \cdot S \cdot M_s \cdot \omega(\cos\alpha \sin^2\theta_{max} \sin 2\omega t + 2 \sin\alpha \sin\theta_{max} \cos\omega t). \quad (10)$$

Thus the skew of the equilibrium axis gives rise to a decrease in second harmonics and an appearance of the fundamental. As is discussed later, the fundamental is eliminated using a filter. Here only the second harmonics is dealt with. For fluctuation of the skew angle α due to the local off-ribbon-axis anisotropy, the integrated value of (10) should be treated in a similar way to (9). If the skew angle α, which is a result of a balance among the anisotropy, magnetostatic, and demagnetizing energies, is kept constant by means of keeping $H_{\parallel} + H_k$ constant, the integrated value of (10) does not change. Thus the skewed equilibrium axis of magnetization rotation does not affect the compensation of anisotropy field.

Experimental Arrangement

The block diagram of the apparatus is shown in Fig. 3. The sense coil into which an amorphous ribbon is inserted is 7 mm X 5 mm X 4 cm in dimensions, and has 1.5×10^4 turns winding. A pair of rectangular coils (1 cm X 1.5 cm X 10 cm) to apply a drive field, which sandwiches the sense coil, are located inside a solenoid. The sense and drive coils are mutually orthogonal. An arrangement of each coil is shown in Fig. 4. The amplitude of drive field is chosen to be 8-19 Oe, where the rotation angle does not exceed 1.5 degree. To apply the tensile stress, weights are suspended by a thread attached on the ribbon end using a pulley. A frequency of drive field is chosen as 4.8 kHz, and the second harmonics are processed by the tuned amplifier whose gain is 55 dB for the second harmonics, and -33 dB for the fundamental, a great part of which arises due to the miss-orthogonality between the sense coil and the drive coils.

We have measured some characteristics of the second harmonics to confirm predictions of (5). The second harmonics for the $Fe_{40}Ni_{40}P_{14}B_6$ ribbon with a cross section of 1.8 mm X 40 μm and the drive field are shown in Fig. 5, where $H_{\parallel} = 70$ Oe, $\sigma = 2.7 \times 10^8$ dyn/cm^2, and $H_{\perp max} = 10$ Oe. Concerning the

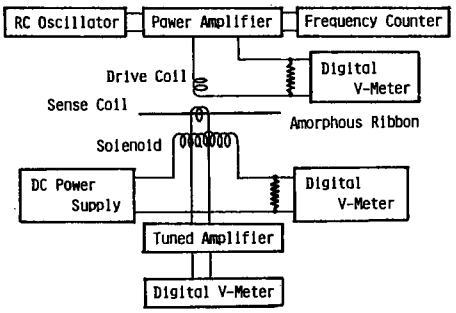

Fig. 3. Block diagram of apparatus.

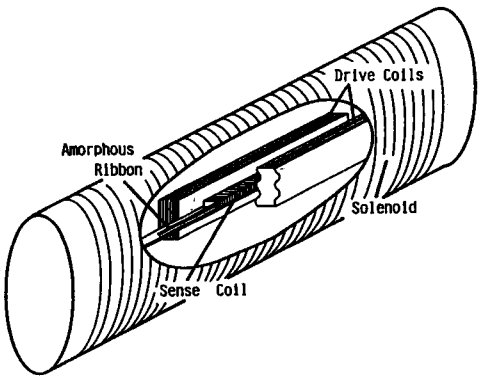

Fig. 4. Arrangement of sense coil, drive coils, and solenoid.

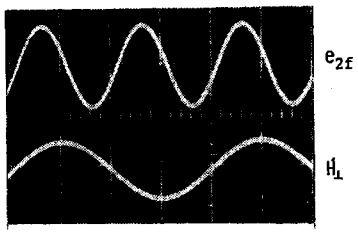

Fig. 5. Photograph of second harmonics and drive field for $Fe_{40}Ni_{40}P_{14}B_6$ ribbon. $H_{\parallel} = 70$ Oe, $H_{\perp max} = 10$ Oe, $\sigma = 2.7 \times 10^8$ dyn/cm^2.

magnitude of the second harmonics, (11) is obtained from (5) and (6),

$$1/\sqrt{e_{2f}} = \frac{1}{\sqrt{2\pi N \cdot S \cdot M_s \cdot \omega}} \cdot \frac{1}{H_{\perp max}} (H_{\parallel} + H_K + H_s). \quad (11)$$

$1/\sqrt{e_{2f}}$ is a linear function of the bias field. In Fig. 6, both e_{2f} and $1/\sqrt{e_{2f}}$ are shown as a function of the dc bias field. Values are normalized with respect to that for a bias field of 25 Oe. The linear relation between $1/\sqrt{e_{2f}}$ and the bias field can be seen for fields higher than 75 Oe where technical saturation seems to be achieved. If the line $1/\sqrt{e_{2f}}$ is extrapolated to the horizontal axis, a shape anisotropy field of about 240 Oe is obtained. The value is higher than that calculated approximately. It may be due to the irregularity of the ribbon surface. The dc bias field dependence of $1/\sqrt{e_{2f}}$ is shown in Fig. 7 taking the magnitude of the drive field as a parameter. A slope of the line can be seen to become steeper with decreasing drive field. As (11) predicts, extrapolated values cross each other at

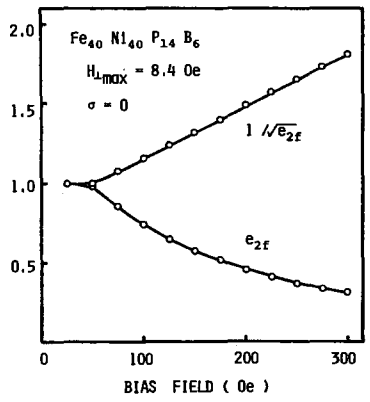

Fig. 6. Normalized e_{2f} and $1/\sqrt{e_{2f}}$ versus bias field for $Fe_{40}Ni_{40}P_{14}B_6$ ribbon.

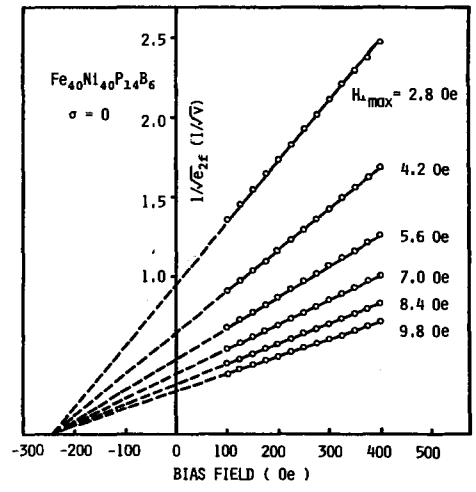

Fig. 7. $1/\sqrt{e_{2f}}$ as function of bias field for $Fe_{40}Ni_{40}P_{14}B_6$ ribbon with amplitude of drive field as parameter.

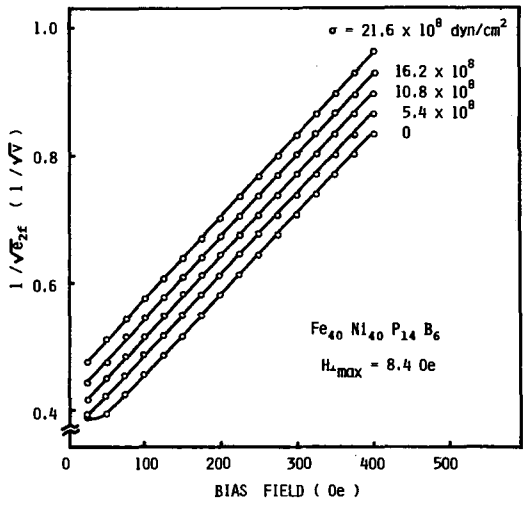

Fig. 8. $1/\sqrt{e_{2f}}$ as function of bias field for $Fe_{40}Ni_{40}P_{14}B_6$ ribbon with tensile stress as a parameter.

the shape anisotropy field. In Fig. 8 $1/\sqrt{e_{2f}}$ is shown as a function of the bias field when the tensile stress is varied. Lines are nearly parallel and shift toward the lower bias field in proportion to the increment in the anisotropy field due to the tensile stress.

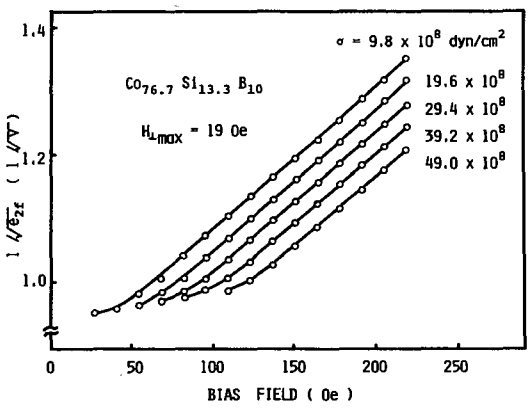

Fig. 9. $1/\sqrt{e_{2f}}$ as function of bias field for $Co_{76.7}Si_{13.3}B_{10}$ ribbon with tensile stress as parameter.

Co based amorphous ribbon has been known to exhibit a negative magnetostriction [1], [2], [7]. Fig. 9 shows the bias field dependence of $1/\sqrt{e_{2f}}$ for the $Co_{76.7}Si_{13.3}B_{10}$ amorphous ribbon with the cross section of 0.5 mm X 20 μm when the tensile stress is varied. Linear relations between $1/\sqrt{e_{2f}}$ and the bias field are seen beyond the saturation field which increases with the tensile stress. It is also seen that the line shifts toward the higher field with increasing tensile stress contrary to the result for $Fe_{40}Ni_{40}P_{14}B_6$ with a positive magnetostriction. Thus the method is also adaptable to the ribbon with the negative magnetostriction. As is seen above, (5) well explains the measured results.

Measured Results

It is necessary to measure the cross sectional area of the specimen to obtain the saturation magnetostriction constant. However, it seems to be difficult to measure it with satisfactory accuracy because of the irregularity of the ribbon surface. Therefore (8) is rewritten as

$$\lambda_s = \frac{1}{3} \cdot \frac{H_k}{T} \cdot \sigma_s \cdot W, \tag{12}$$

where σ_s is the specific magnetization at room temperature (emu/g), T is the value of weight suspended on the ribbon end (dyn), and W is the weight per unit length of the specimen (g/cm). These values are conventionally measurable.

The applied tensile stress (T) dependence of anisotropy field for both $Fe_{40}Ni_{40}P_{14}B_6$ (1.8 mm X 40 μm in cross section) and $Fe_{80}B_{20}$ (1.3 mm X 30 μm) are shown in Fig. 10. These dependences are linear and give the saturation magnetostrictions of 12.3 X 10^{-6} and 34.6 X 10^{-6}, respectively. The values are compared with those measured using strain gauges by Egami *et al.* [8] and by O'Handley *et al.* [9] in Table I. Present values are about ten percent higher than the reported values. Fig. 11 shows the variation of anisotropy field for the $Co_{76.7}Si_{13.3}B_{10}$ ribbon as a function of tensile stress. The slope gives the saturation magnetostriction λ_s of -4.1 X 10^{-6}.

The accuracy and sensitivity of the measuring method are considered as follows. According to (12) it is necessary to measure three kinds of values, namely H_k/T, σ_s, and W, to determine the saturation magnetostriction λ_s. It is possible to measure the saturation magnetization σ_s within the error

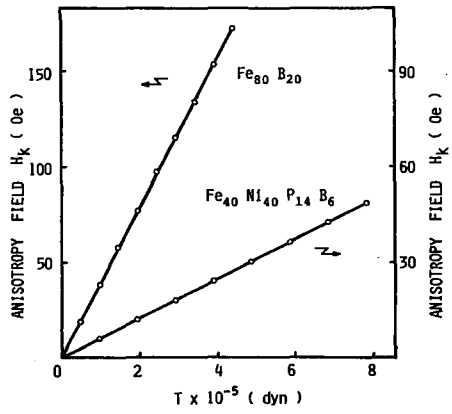

Fig. 10. Anisotropy field as function of tensile stress (T) for $Fe_{40}Ni_{40}P_{14}B_6$ and $Fe_{80}B_{20}$ ribbons.

TABLE I
SATURATION MAGNETOSTRICTIONS λ_s IN COMPARISON WITH THOSE REPORTED ALREADY

Alloy	λ_s x 10^6	
Metglas 2826 ($Fe_{40}Ni_{40}P_{14}B_6$)	11 [8],	12.3 *
Metglas 2605 ($Fe_{80}B_{20}$)	31 [9],	34.6 *

* Present work

of ±1 percent by using a vibrating sample magnetometer. The amount of scatter of the measured H_k/T was within ±2 percent, which might originate from the mechanical friction of the pulley. The weight per unit length of the ribbon W is measurable with the error less than ±2 percent by a conventional method. From these values, it is estimated that the error in determination of λ_s does not exceed ±5 percent.

The change in e_{2f} from the value with no applied stress, which is caused by the small change of ΔH_k, is derived from (5) and (6) as

$$\Delta e_{2f} = -4\pi \cdot N \cdot S \cdot M_s \cdot \omega \cdot \frac{H_{\perp\max}^2}{(H_{\parallel} + H_s)^3} \cdot \Delta H_k. \tag{13}$$

If we consider λ_s to be a variable for our convenience, a relation

$$\frac{\Delta e_{2f}}{\Delta \lambda_s} = -12\pi \cdot T \cdot N \cdot \omega \cdot \frac{H_{\perp\max}^2}{(H_{\parallel} + H_s)^3} \tag{14}$$

is obtained by substitution of (8) into (13), where $T = \sigma \cdot S$ is used. The conversion ratio $\Delta e_{2f}/\Delta\lambda_s$ depends on the shape anisotropy field. For Metglas $Fe_{40}Ni_{40}P_{14}B_6$ ribbon with 1.8 mm X 40 μm X 12 cm in dimensions, the application of the weight of 1.6 kg (possible maximum value for the present apparatus), when $H_{\perp\max} = 8.4$ Oe and $H_{\parallel} = 300$ Oe, causes the change of 1.0 mV in e_{2f}, which corresponds to the saturation

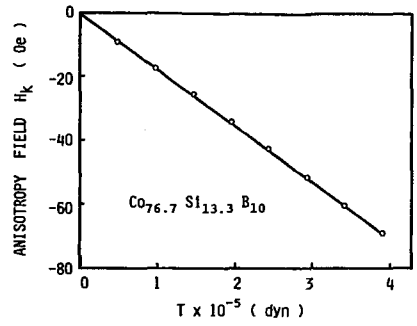

Fig. 11. Anisotropy field as function of tensile stress (T) for $Co_{76.7}Si_{13.3}B_{10}$ ribbon.

magnetostriction of 12.3 X 10^{-6}. The resolution of the tuned amplifier employed is about 20 μV. Consequently, the maximum sensitivity is estimated to be about 2 X 10^{-7}.

CONCLUSION

The present method utilizing the small-angle magnetization rotation has been proved to be useful, because of simplicity and high sensitivity, for the magnetostriction measurement of splat-cooled amorphous ribbons. The estimated error in the measurement is less than five percent. The sensitivity of the method is about 2 X 10^{-7} for Metglas $Fe_{40}Ni_{40}P_{14}B_6$ ribbon. It is possible to increase the sensitivity by increasing the frequency of ac drive field.

ACKNOWLEDGMENT

The authors are thankful to Dr. S. Konishi for suggesting the present work and helpful discussion, and to Dr. T. Yamaguchi for helpful discussion.

REFERENCES

[1] R. C. O'Handley, "Magnetostriction of metallic glasses," in *Amorphous Magnetism II*, R. A. Levy and R. Hasegawa, Eds. New York: Plenum, 1977, pp. 379-392.
[2] H. A. Brooks, "Magnetostriction vs Co content in amorphous alloys of Fe-Co-P-B-Al," *J. Appl. Phys.*, vol. 47, pp. 344-345, 1976.
[3] N. Tsuya, K. I. Arai, Y. Shiraga, M. Yamada, and T. Masumoto, "Magnetostriction of amorphous $Fe_{0.80}P_{0.13}C_{0.07}$ ribbon," *Phys. Stat. Sol. (A)*, vol. 31, pp. 557-561, 1975.
[4] S. Konishi, S. Sugatani, and Y. Sakurai, "A high-speed NDRO analog memory using electrodeposited permalloy wires," *IEEE Trans. Magn.*, vol. MAG-5, pp. 14-18, 1969.
[5] F. E. Luborsky, J. J. Becker, and R. O. McCary, "Magnetic annealing of amorphous alloys," *IEEE Trans. Magn.*, vol. MAG-11, pp. 1644-1649, 1975.
[6] T. Egami and P. J. Flanders, "Temperature dependence of 'magnetic anisotropy' in amorphous alloys," in *AIP Conf. Proc.*, no. 29, pp. 220-221, 1976.
[7] H. Fujimori, K. I. Arai, H. Shiraga, H. Saito, T. Masumoto, and N. Tsuya, "Magnetostriction of Fe-Co amorphous alloys," *Japan J. Appl. Phys.*, vol. 705-706, 1976.
[8] T. Egami, P. J. Flanders, and C. D. Graham, Jr., "Amorphous alloys as soft magnetic meterials," in *AIP Conf. Proc.*, no. 24, pp. 697-701, 1975.
[9] R. C. O'Handley, L. I. Mendelsohn, R. Hasegawa, R. Ray and S. Kavesh, "Low-field magnetic properties of $Fe_{80}B_{20}$ glass," *J. Appl. Phys.*, vol. 47, pp. 4660-4662, 1976.